A Monte Carlo Simulation Model for Radiation Dose to Metastatic Skeletal Tumor from Rhenium-186(Sn)-HEDP

R. Chandrasiri Samaratunga, Stephen R. Thomas, Jerry D. Hinnefeld, Larry C. Von Kuster, David M. Hyams, Jonathan S. Moulton, Matthew I. Sperling and Harry R. Maxon III

Divisions of Radiological Sciences, Nuclear Medicine and Diagnostic Radiology, Department of Radiology and Departments of Surgery and Pathology, University of Cincinnati Medical Center, Cincinnati, Ohio

A Monte Carlo model has been developed for simulation of dose delivery to skeletal metastases by the bone surface-seeking radiopharmaceutical ^{186}Re (Sn)-HEDP. **Methods:** The model simulates: (1) the heterogeneous small scale geometry of the soft tissue/bone-spicule structure in the lesions as determined by histomorphometric measurements of histologic specimens, (2) the small scale spatial distribution of the radiopharmaceutical on the lesion bone spicule surface as determined by autoradiography, and (3) the ^{186}Re beta and conversion electron decay spectrum and the associated charged particle transport within the modeled geometries. The results are compared with the commonly employed uniform lesion model, which assumes: (1) homogenous lesion morphology, (2) uniform distribution of radioactivity within the lesion, and (3) complete energy deposition by charged particles within the lesion due to decay of this activity. Gamma and x-ray photons from the ^{186}Re spectrum were assumed to escape from the lesion volume in both models. **Results:** Results show a significant dependence on the bone volume fraction and hence on the histology of the lesion (lytic, blastic or mixed). The uniform lesion model calculations underestimate the radiation dose to blastic lesions by as much as a factor of 1.8. However, for lytic lesions with low bone volume fractions, both models provide similar dose values. **Conclusions:** These new model calculations provide a mechanism for optimizing treatment planning and dose response evaluations of therapeutic bone-seeking radiopharmaceuticals.

Key Words: Monte Carlo model; skeletal metastases; radiation dose; bone surface-seeking radiopharmaceutical; rhenium-186(Sn)-HEDP

J Nucl Med 1995; 36:336–350

M ultifocal bone metastases associated with advanced cancers are often accompanied by severe pain. External radiation therapy can provide significant palliation for 50%–80% of patients. However, when skeletal involve-ment is widespread, such therapy is limited even with regional hemibody fields (1). As an alternative, internal radiotherapy using bone-seeking, beta-emitting radiopharmaceuticals has received increased attention in recent years (2,3). Preferential accumulation of the radiopharmaceuticals in the metastatic lesion sites in bone also has a significant advantage in limiting the dose to other organs. Successful palliation with minimal red marrow toxicity has been achieved with several radiopharmaceuticals such as ^{186}Re-hydroxyethylidene diphosphonate (^{186}Re(Sn)-HEDP) (4,5), ^{153}Sm-ethylene-diamine-tetramethylene-phosphonate (EDTMP) (4,6,7), ^{131}I-α-amino-(4-hydroxybenzylidene)-di-phosphonate (BDP3) (8), ^{89}Sr-chloride (9), ^{32}P-sodium orthophosphate (10), ^{90}Y-citrate (11) and stannic diethyl-ene-triamine-pentaacetic acid (^{117m}Sn(IV)-DTPA) (12). However, little is known about the radiodosimetry of these compounds at the microscopic level. Such knowledge is fundamental to their optimal use for treatment of skeletal metastases.

Bone spicules and soft tissue (metastatic tumor cells and/or marrow) constitute the two distinct tissue compo-nents in skeletal lesions. In general, three basic types of skeletal metastases are identified: (1) osteoblastic lesions with a high mineralized bone content, (2) osteolytic lesions with a high soft-tissue content, and (3) mixed osteoblastic/ osteolytic lesions. The radiation dose to the tumor cells, i.e., the soft tissue component in the lesion, is the impor-tant parameter for dose response considerations. The most commonly employed dosimetry model, termed the uniform lesion model in this discussion, provides only a first order of approximation based on the assumptions of: (1) homog-enous lesion morphology, (2) uniform distribution of radio-activity within the lesion, and (3) complete energy deposi-tion within the lesion by charged particles.

F. W. Spiers, J. R. Whitwell, A. H. Beddoe and P. J. Darley pioneered the evaluation of beta dose in trabecular bone based on path length distributions in bone and soft tissue (13–16). Beta-ray dose to soft tissue was evaluated by utilizing the beta-ray range-energy relationship $R = aE^m$ (R: range; E: energy; a, m: constants) in the Monte Carlo simulation of energy deposition by beta-rays arriving in a

soft tissue cavity. Path lengths for alternate traversal of soft tissue/bone spaces before arriving in a given cavity were sampled from the appropriate distributions.

We present a Monte Carlo simulation model for the systematic assessment of radiation dose to the soft tissue component of skeletal metastases based on the morphologic properties of the three basic lesion types and the actual radionuclide uptake patterns within the bone spicules for [186]Re-HEDP. The path length distributions in the soft tissue and bone components of the skeletal metastases were obtained using methods different from those described by Whitwell and Spiers (13,15). Therefore the path length distributions were utilized differently in our Monte Carlo model (see below in METHODS). The model, termed the heterogenous lesion model, simulated: (1) the heterogeneous small scale geometry of the soft tissue/bone-spicules structure in the lesions as determined by histomorphometric measurements of histologic specimens, (2) the small scale spatial distribution of the radiopharmaceutical on the lesion bone spicule surface as determined by autoradiography, and (3) the radioactive emissions of the [186]Re decay spectrum and the associated charged particle transport within the modeled geometries. The results provide new information on variations in dose to the soft tissue component in skeletal lesions as a function of lesion type.

METHODS

Autoradiography

Bone biopsies from one metastatic site in each of seven patients were obtained 3.5 ± 1.6 hr following an intravenous therapeutic administration of 34.7 ± 0.6 mCi of [186]Re(Sn)-HEDP. Informed consent both for the therapy and for the biopsy was obtained according to the guidelines of the Institutional Review Board of the University of Cincinnati. All biopsy specimens were obtained from lesions that had been targeted for in vivo quantification. All biopsies were performed using a Craig needle under sterile conditions. The biopsies were weighed and counted in a gamma counter with 50–200-keV windows. Sections approximately 0.5 μm thick were then cut with a microtome. The cut sections were adhered to clean glass slides, dried and immersed in a melted photographic emulsion at 43°C. Emulsions of Kodak NTB-2 (Ilford, Inc., Paramus, NJ) and/or Ilford G5 (Eastman Kodak, Rochester, NY), diluted 1:1 with water, were used for this purpose. After the slides were coated with the emulsion, they were allowed to dry slowly for several hours to avoid emulsion cracking or shifting. The slides with exposed emulsions and control slides with no activity (obtained separately from sections of normal rabbit femurs under a protocol approved by the Institutional Animal Care and Use Committee of the University of Cincinnati) were developed using Kodak D-19 developer diluted 1:1 with water and undiluted Kodak fixer. The developed sections were stained with toluidine blue, rinsed with distilled water and cleared with xylene before applying the coverslips.

Autoradiographs were digitized and evaluated with a Magiscan image analysis system (Magiscan M2D, Joyce-Loebl Ltd., New Castle, United Kingdom) to determine the radionuclide deposition characteristics in lesions. A protocol was established for choosing spicule surface, interior and soft tissue regions for analysis, background subtraction and excluding areas of anomalous optical den-

sity (artifacts). The optical density in the emulsion due to exposure from ionizing radiation in the underlying sample provides a representation of radionuclide distribution. Surface deposition up to a depth δ of approximately 10 μm into the bone spicules was observed in all seven lesions. A typical autoradiograph is shown in Figure 1. Radionuclide uptake is seen as high optical density areas at the soft tissue (tumor) and bone-spicule interfaces. The ratio of the activity a_δ deposited in the $\delta = 10$ μm bone layer to the total activity a_{tot} deposited in the whole sample was evaluated according to:

$$\frac{a_\delta}{a_{tot}} = \frac{1}{1 + \dfrac{R_a \cdot R_v}{R_{sv} \cdot \delta}}, \qquad \text{Eq. 1}$$

where R_a is the ratio of the optical density in the soft tissue-to-optical density in bone layer, R_v is the ratio of the soft tissue volume-to-bone volume and R_{sv} is the ratio of the bone surface area-to-bone volume.

Histomorphometry

Histomorphometric studies were performed on 25 archived pathology samples from skeletal metastases in 24 patients with prostate, breast or lung cancer. The lesions were classified as lytic (7), blastic (14), mixed (3) and normal (1). Von Kossa stained, 0.5- to 1-μm thick histologic sections were studied microscopically utilizing a Merz Grid eyepiece reticle (Fig. 2). Using standard histomorphometric techniques (17), the three-dimensional geometric properties were deduced from the two-dimensional measurements based on the assumption of three-dimensional isotropy. The measurements described below were performed with semi-automatic image analysis software (Bioquant®, Nashville, TN) using a computer linked to a light microscope.

Path length distributions $f_s(l)$ and $f_b(l)$ in soft tissue (tumor) and mineralized bone spaces for each specimen were determined from random measurements of path lengths l_s and l_b in the respective media. The random locations were determined by the intersections of the Merz grid with the bone spicule surfaces (Fig. 2). A soft tissue path length l_s was defined as the distance in soft tissue, measured from a random location on a bone spicule surface to a neighboring bone spicule. The mineral path length l_b was defined
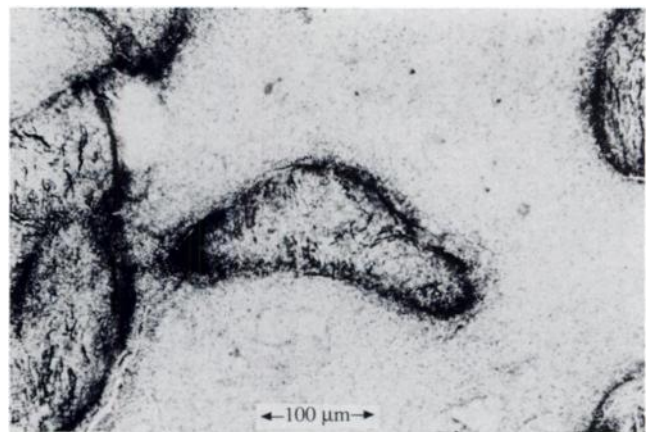

FIGURE 1. Autoradiograph of a section through a needle biopsy of a rib metastasis from prostate cancer obtained 3 hr after treatment of the patient with [186]Re-HEDP. High optical density areas on bone spicule surfaces (dark bands) represent radionuclide deposition up to a depth of approximately 10 μm (magnification factor = 62.5).

as the bone spicule width at the same location. Both path lengths were measured perpendicular to the bone/soft tissue boundary at the random location. Typical path length distributions $f_a(l)$ and $f_b(l)$ for one lesion sample are shown in Figure 3. Table 1 lists the mean path lengths and the standard deviations for the 25 lesion samples.

In addition to the path length distributions, the following geometric parameters were estimated (Table 1).

Bone volume fraction in the sample:

$$f_{Vb} = V_b/(V_b + V_s), \qquad \text{Eq. 2}$$

where V_b is bone volume and V_s is soft tissue volume.

Total bone surface to total bone volume ratio:

$$\frac{A_b}{V_b} = \frac{\displaystyle\sum_{spicules} a_i}{\displaystyle\sum_{spicules} v_i}, \qquad \text{Eq. 3}$$

where a_i is the surface area of the ith spicule and v_i is the volume of the ith spicule.

Lesion Dosimetry: General Considerations Based on MIRD Schema

Radiopharmaceutical dosimetry based on the Medical Internal Radiation Dose (MIRD) schema (18) is represented by the generic equation:

$$D_{target} = \sum_{source} S_{target \leftarrow source} \cdot \tau_{source}. \qquad \text{Eq. 4}$$

Here D_{target} (Gy/Bq) is the dose to the target region or organ per unit administered activity of the radionuclide. The S value $S_{target \leftarrow source}$ (Gy/Bq s) has the form:

$$S_{target \leftarrow source} = \frac{\displaystyle\sum_i \Delta_i \cdot \varphi_{i,target \leftarrow source}}{m_{target}} = \frac{\Delta \cdot \varphi_{target \leftarrow source}}{m_{target}}, \qquad \text{Eq. 5}$$

$$\Delta = \sum_i \Delta_i, \qquad \text{Eq. 6}$$

$$\varphi_{target \leftarrow source} = \frac{\displaystyle\sum_i \Delta_i \cdot \varphi_i}{\displaystyle\sum_i \Delta_i}, \qquad \text{Eq. 7}$$

where Δ_i is the mean energy per particle of type i radiation with energy E_i; $\varphi_{i,target \leftarrow source}$ is the absorbed fraction of radiation in the target with energy E_i; m_{target} is the mass of the target region, Δ is the total mean energy per nuclear transition and $\varphi_{target \leftarrow source}$ is the mean absorbed fraction in the target per nuclear transition.

Typically, anatomically distinct regions (organs) are considered as sources. The cumulated activity in a given source region per unit administered activity known as the residence time, τ_{source}, is:

$$\tau_{source} = \frac{1}{a_0} \int a_{source}(t) \, dt, \qquad \text{Eq. 8}$$

where a_0 is the administered activity and $a_{source}(t)$ is the activity in the source as a function of time. Residence time is dependent on the radioactivity uptake within the source region, the time scale
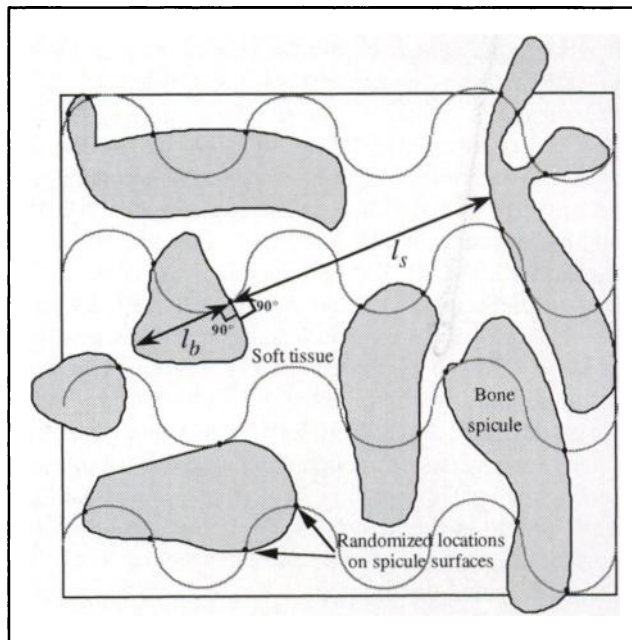

FIGURE 2. Schematic of a microscopic section through a skeletal metastasis with superimposed Merz grid. l_b: Path length in bone. l_s: Path length in soft tissue. The path length measurement locations l are randomized by the intersections of the half circles in the Merz grid with the spicule surfaces. The path lengths are measured perpendicular to the bone/tissue interface at each intersection.

associated with biologic turnover and the half-life of the radionuclide decay.

In the case of ^{186}Re (Sn)-HEDP, the dose to the soft tissue component (tumor) in the lesion is almost entirely delivered by the short-range beta minus particles and conversion electrons (~1 mm in soft tissue, ~0.5 mm in bone for the average beta minus energies). Therefore, for lesion dosimetry, the lesion itself is considered as the source region and Equation 4 simplifies to:

$$D_s = S_{s \leftarrow l} \cdot \tau_l = \frac{\Delta \cdot \phi_{s \leftarrow l}}{m_s} \cdot \tau_l, \qquad \text{Eq. 9}$$

where the subscripts l and s denote the lesion and the soft tissue component in the lesion respectively.

Dose to Tumor: The Uniform Lesion Model. The assumptions employed for the commonly used uniform model, with source equal to target, invoke absorbed fractions $\varphi_{i,target \leftarrow source}$ of unity for charged particles and of zero for photons. Therefore, D_s simplifies to:
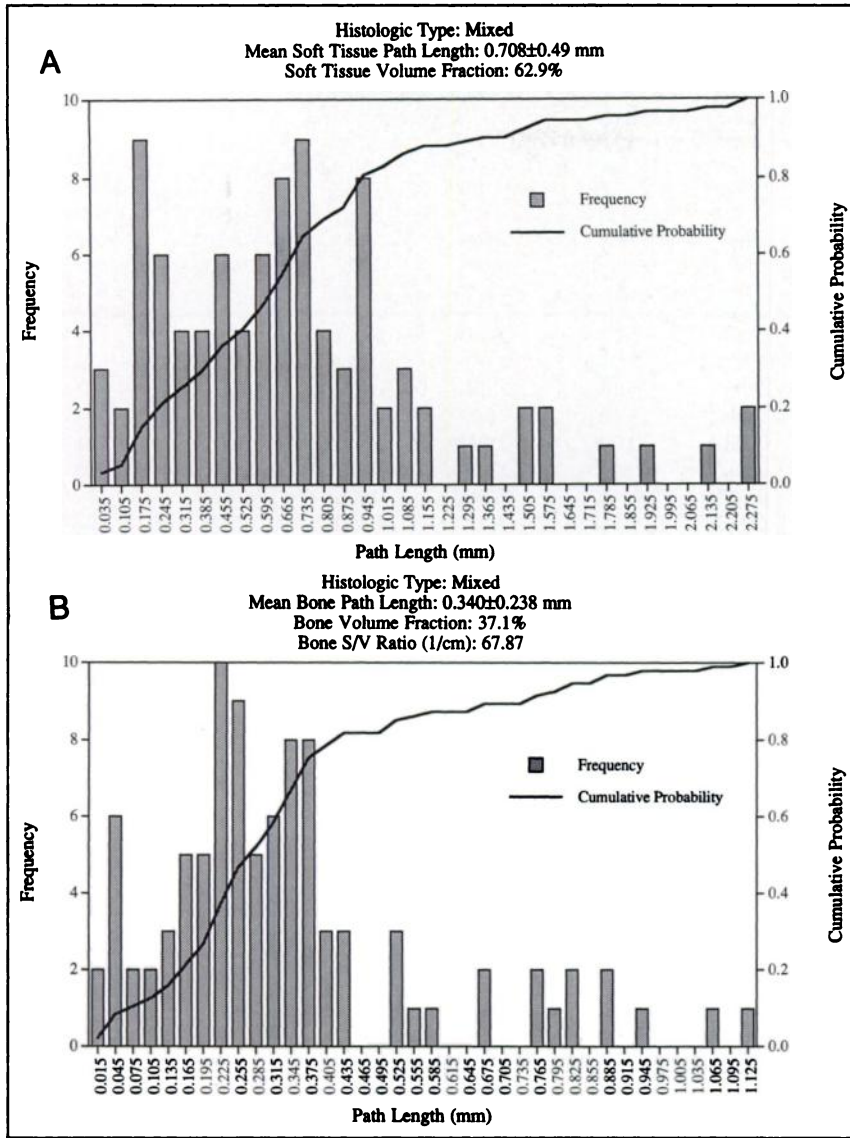
$$D_s = S_{unif} \tau_l, \qquad \text{Eq. 10}$$

where:

$$S_{unif} = \frac{\displaystyle\sum_{\substack{charged \\ particles}} \Delta_i}{m_l} = \frac{\displaystyle\sum_{\substack{charged \\ particles}} \Delta_i}{\rho_l V_l}, \qquad \text{Eq. 11}$$

$$\rho_l = \rho_b f_{Vb} + \rho_s f_{Vs}, \qquad \text{Eq. 12}$$

where m_l is the mass of lesion; V_l is the volume of lesion; ρ_l, ρ_s and ρ_b are the densities of lesion, soft tissue and bone respectively; f_{Vb} is the bone volume fraction; and f_{Vs} ($= 1 - f_{Vb}$) is the soft tissue volume fraction. For ^{186}Re,

FIGURE 3. (A) Soft-tissue path length distribution of lesion sample no. 17 (Table 1). (B) Bone path length distribution of lesion sample no. 17 (Table 1). These distributions are used in the Monte Carlo simulation of the heterogenous lesion model.

$$\sum_{\substack{\text{charged} \\ \text{particles}}} \Delta_i = 5.49 \times 10^{-14} \frac{Gy \cdot kg}{Bq \cdot s}.$$

Dose to Tumor: The Heterogenous Lesion Model. In the heterogenous model, the soft tissue and bone components of the metastatic lesions may be considered as two distinct source regions, with soft tissue as the target region. The absorbed fractions $\phi_{s \leftarrow s}$ and $\phi_{s \leftarrow b}$ are not assumed to be equal to unity for charged particles. However, as in the case of the uniform lesion model, the absorbed fractions due to photons are taken to be zero (gamma rays and x-rays are assumed to escape the lesion volume). For the heterogenous model, Equation 9 therefore needs to be rewritten as follows:

$$D_s = S_{s \leftarrow s} \cdot \tau_s + S_{s \leftarrow b} \cdot \tau_b, \qquad \text{Eq. 13}$$

where:

$$\tau_l = \tau_b + \tau_s, \qquad \text{Eq. 14}$$

and the subscript b denotes bone-spicules in the lesion.

The autoradiographic study results described below have revealed a nonuniform distribution of ^{186}Re-HEDP within the le-

sions, mainly confined to surface deposition on bone spicules. This implies $\tau_s \approx 0$ and $\tau_l \approx \tau_b$. Therefore, with the assumptions that $\tau_s = 0$, and $\tau_b = \tau_l$ Equation 13 may be further simplified to:

$$D_s = S_{s \leftarrow b} \cdot \tau_l, \qquad \text{Eq. 15}$$

$$S_{s \leftarrow b} = \frac{\Delta \cdot \phi_{s \leftarrow b}}{m_s} = \frac{\Delta \cdot \phi_{s \leftarrow b}}{\rho_s \cdot f_{Vs} \cdot V_l}, \qquad \text{Eq. 16}$$

where m_s is the mass of soft tissue component and Δ and $\phi_{s \leftarrow b}$ are determined according to Equations 6 and 7 with the summation over i restricted to charged particles only, i.e.,

$$\Delta = \sum_{\substack{\text{charged} \\ \text{particles}}} \Delta_i = 5.49 \times 10^{-14} \frac{Gy \cdot kg}{Bq \cdot s} \quad \text{and}$$

$$\phi_{s \leftarrow b} = \frac{\sum\limits_{\substack{\text{charged} \\ \text{particles}}} \Delta_i \cdot \phi_{i,s \leftarrow b}}{\sum\limits_{\substack{\text{charged} \\ \text{particles}}} \Delta_i}.$$

TABLE 1
Statistical Parameters of 25 Lesion Samples of Skeletal Metastases in 24 Patients

| Sample no.	Histologic classification	Sample size (no. of path length pairs in soft tissue and bone)	Soft-tissue path length distribution Mean (mm) $\bar{l}_s$	s.d. (mm) Δl_s	Bone path length distribution Mean (mm) $\bar{l}_b$	s.d. (mm) Δl_b	Bone volume fraction f_{vb}	Bone surface area per unit bone volume (cm^{-1}) A_b/V_b
1	B	182	0.098	0.074	0.040	0.026	0.350	764.2
2	B	139	0.190	0.130	0.161	0.123	0.531	179.1
3	B	101	0.190	0.194	0.136	0.099	0.360	237.9
4	B	103	0.211	0.128	0.149	0.100	0.327	254.0
5	B	142	0.220	0.225	0.169	0.131	0.421	201.4
6	B	395	0.247	0.150	0.065	0.062	0.198	468.5
7	B	174	0.247	0.181	0.090	0.071	0.288	394.0
8	B	137	0.256	0.212	0.128	0.092	0.426	232.0
9	B	126	0.264	0.247	0.129	0.090	0.409	338.5
10	B	192	0.265	0.253	0.137	0.121	0.325	279.0
11	B	124	0.341	0.386	0.183	0.142	0.384	190.9
12	B	94	0.462	0.685	0.167	0.274	0.185	375.8
13	B	98	0.483	0.526	0.113	0.095	0.192	426.1
14	B	61	0.758	0.579	0.261	0.160	0.261	146.6
15	M	88	0.406	0.334	0.177	0.153	0.304	229.4
16	M	72	0.653	1.571	0.100	0.082	0.207	150.9
17	M	94	0.708	0.486	0.340	0.238	0.371	67.9
18	N	147	0.594	0.339	0.192	0.162	0.253	158.1
19	L	80	0.771	0.703	0.148	0.115	0.141	316.1
20	L	66	0.790	0.051	0.087	0.051	0.115	322.7
21	L	69	0.834	0.392	0.135	0.086	0.161	324.4
22	L	129	1.013	0.716	0.135	0.108	0.150	211.5
23	L	64	1.034	0.528	0.186	0.124	0.218	220.1
24	L	53	1.116	0.692	0.226	0.270	0.222	158.1
25	L	32	1.329	0.816	0.090	0.035	0.063	398.0

L = lytic; B = blastic; M = mixed; and N = normal.

TABLE 2
Summary of ^{186}Re Spectrum (Half-life-90.64 hr)

Radiation type	Energy (MeV) E_i	Particles transition n_i	$\dfrac{\text{Mean energy}}{\text{particle type}}$ (Gy kg/Bq s) $\Delta_i = n_i \cdot E_i$	%Δ_i
β_3^-	0.309 (mean) 0.934 (maximum)	0.21	1.04×10^{-14}	17.8%
β_4^-	0.362 (mean) 1.072 (maximum)	0.73	4.23×10^{-14}	72.5%
10 conversion electrons	From 0.05 to 0.125	0.14	2.33×10^{-5}	4.0%
γ_1 (Os)*	0.137	0.087	1.91×10^{-15}	3.3%
γ_1 (W)	0.123	0.018	3.54×10^{-16}	0.6%
15 x-rays and 2 gamma rays	From 0.008 to 0.768	0.136	1.037×10^{-15}	1.8%
	Total	$\sum n_i = 1.32$	$\sum \Delta_i = 5.83 \times 10^{-14}$	100%
			$\sum\limits_{\text{charged particles}} \Delta_i = 5.49 \times 10^{-14}$	

*The 0.137 MeV gamma ray is used in quantitative in vivo radionuclide imaging.
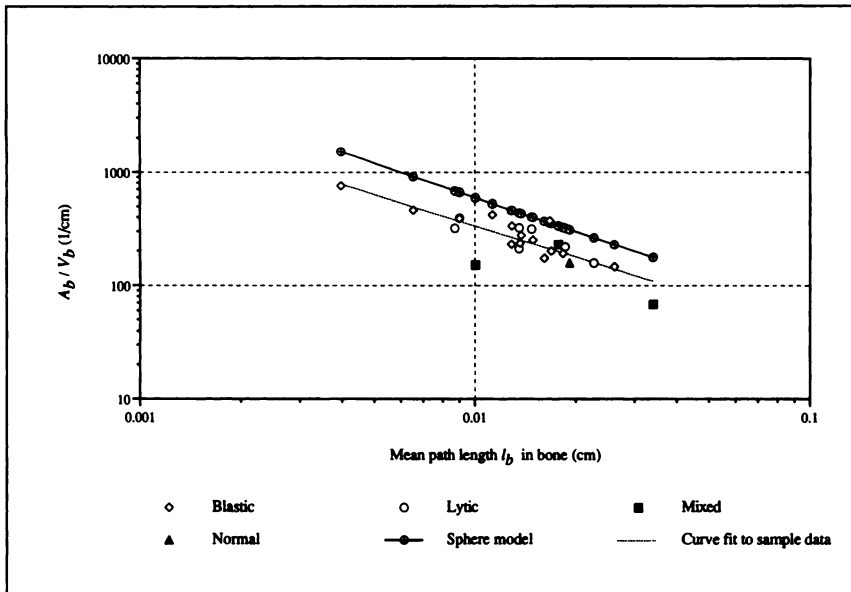
FIGURE 4. Bone surface-to-bone volume ratio $[A_b/V_b]$ as a function of mean path length $\bar{l}_b$ in bone for 25 lesion samples. Dashed line is the curve fit to sample data: $[A_b/V_b] = 4.9 \times \bar{l}_b^{-0.92}$, Solid line is the model for spheres with diameters equal to $\bar{l}_b$: $[A_{sp}/V_{sp}] = 6.0 \times \bar{l}_b^{-1}$.

Equations 10 and 15 both require knowledge of the lesion residence time τ_l in order to evaluate dose. Rhenium-186 emits a 137-keV gamma radiation suitable for quantitative radionuclide imaging which allows reliable estimates of τ_l to be made for [186]Re-HEDP utilizing sequential in vivo quantitative counting techniques (19). Therefore, the dose comparison between the uniform and the heterogenous lesion models amounts to a comparison of their respective S values according to the equations given below:

$$S_{unif} = \left[\frac{\Delta}{\rho_b \cdot f_{Vb} + \rho_s \cdot f_{Vs}}\right]\frac{1}{V_l} = [S_{unif}]_{unit\ lesion\ volume} \cdot \frac{1}{V_l},$$

Eq. 17

$$S_{s \leftarrow b} = \left[\frac{\Delta \cdot \phi_{s \leftarrow b}}{\rho_s \cdot f_{Vs}}\right]\frac{1}{V_l} = [S_{s \leftarrow b}]_{unit\ lesion\ volume} \cdot \frac{1}{V_l}.$$

Eq. 18

According to Equations 17 and 18, the S value decreases with increasing lesion volume. However, in evaluating dose using Equations 10 or 15, this decrease in S value is compensated for by the increased residence time τ_l associated with the higher uptake of radioactivity in lesions with larger volumes.

The Monte Carlo simulation incorporates the dependence of $\phi_{s \leftarrow b}$ in Equation 18 on the morphologic properties of the lesions through utilization of the path length distributions $f_s(l)$ and $f_b(l)$ from the lesion samples (histomorphometric measurements) and the radionuclide uptake patterns for [186]Re (Sn)-HEDP within the bone spicules (autoradiographic measurements).
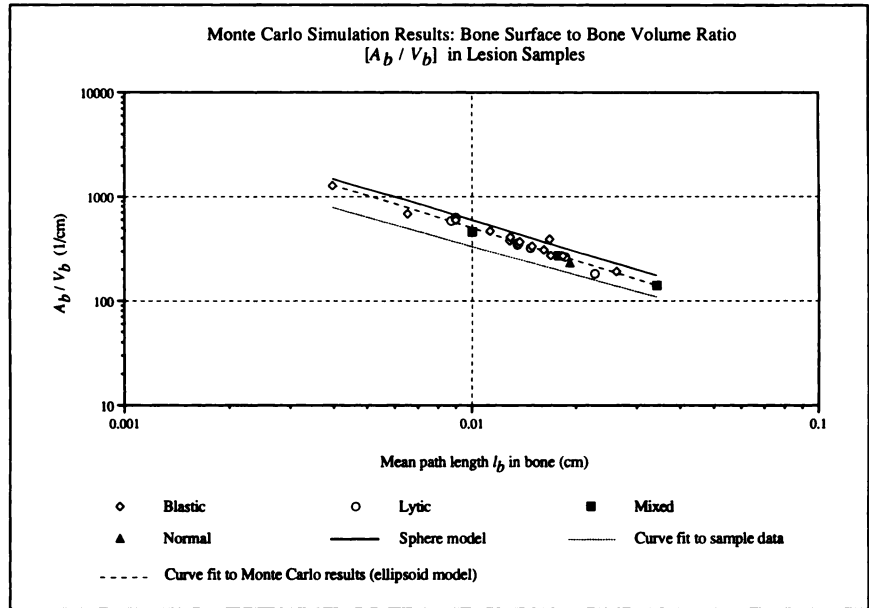
Complex geometries require considerable computational overhead and maintenance of complex data structures during program execution. Therefore, as a first step, we have developed a simple geometric model for bone spicules described below and an algorithm (Appendix A) with minimal complexity and computational overhead for particle transport within this geometric model. The algorithm was based on the use of EGS4/PRESTA (20,21) Fortran code system for coupled transport of electrons and photons.

Monte Carlo Simulation

Rhenium-186 Spectrum. A summary of the [186]Re spectrum is shown in Table 2. Energies of β_3^- and β_4^- particle were sampled from beta minus spectra with endpoint energies 0.934 and 1.072, respectively. The beta minus spectra were constructed using the specifications provided by Prestwich et al. (22). For the remaining radiations, the energies provided by Weber et al. (23) were used. The probability distribution for observing a given radiation type was constructed utilizing previously published data (23). The gamma and the x-ray photons contributing 3.9% and 1.8%, respectively, to the energy/transition were discarded when sampled from the spectrum (i.e., assumed to escape the lesion volume). The absorbed fractions $\phi_{s \leftarrow b}$ and $\phi_{b \leftarrow b}$ were evaluated with respect to the total energy of the charged particles released in the simulation of the [186]Re spectrum. The Bremsstrahlung photons produced by the charged particles were also discarded (rare at low energies).
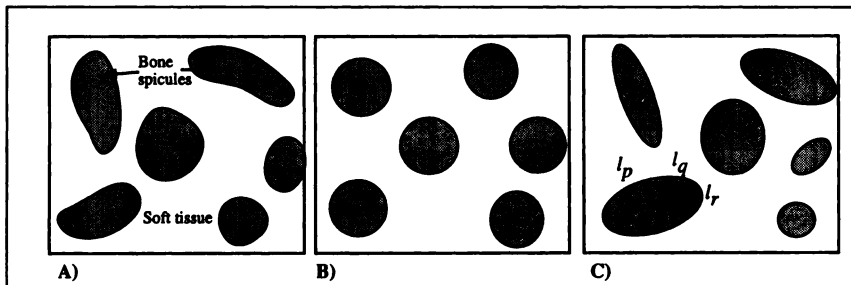
FIGURE 5. Sphere and ellipsoid models for the representation of bone spicules in skeletal lesions. (A) Skeletal lesion with a path length distribution $f_b(l)$ and a mean path length in bone $\bar{l}_b$ in bone as defined in text and Figure 2. (B) Bone spheres with diameter $d = \bar{l}_b$. (C) Bone ellipsoids with axes $l_p l_q$, l_r sampled from the both path length distribution $f_b(l)$.

Monte Carlo Simulation Results: Bone Surface to Bone Volume Ratio
$[A_b / V_b]$ in Lesion Samples

FIGURE 6. Bone surface-to-bone volume ratio $[A_b/V_b]$ for the ellipsoid model. Sphere model: $[A_b/V_b]_{sp} = 6 \times \bar{l}_b^{-1}$. Curve fits: (i) Measured: $[A_b/V_b]_m = 4.9 \times \bar{l}_b^{-0.92}$ and (ii) Monte Carlo simulated ellipsoids: $[A_b/V_b]_{sim} = 4.2 \times \bar{l}_b^{-1.04}$.

Bone Spicule Geometry Model. A simple geometric model for the bone spicules was developed based on the empirical observation of a power law relationship between the lesion geometry parameters $[A_b/V_b]$ and $\bar{l}_b$ (Fig. 4); namely,

$$\frac{A_b}{V_b} \approx k_b \cdot \bar{l}_b^{-n} \quad (k_b = 4.9, \, n = 0.92). \qquad \text{Eq. 19}$$

This relationship is similar to that obeyed by a sphere with diameter d:

FIGURE 7. Monte Carlo transport of radiation in a multiple bone ellipsoid environment. Distances l_s, l_{s1} etc. are sampled from the soft-tissue path length distribution. Ellipsoid dimensions are sampled from the bone path length distribution. If the particle location reaches a perpendicular distance l_s from the starting ellipsoid it is assumed to enter another ellipsoid. Subsequently, if the particle reaches a perpendicular distance l_{s1} from the second ellipsoid it is assumed to enter a third ellipsoid (see text for details). Distances l_s, l_{s1} etc. are oriented perpendicular to the ellipsoid surfaces to be consistent with the histomorphometric measurement method in lesion samples.

$$\left[\frac{A}{V}\right]_{sp} \approx k_{sp} \cdot d^{-n} \quad (k_{sp} = 6.0, \, n = 1). \qquad \text{Eq. 20}$$

$[A/V]_{sp}$ for $d = \bar{l}_b$ is plotted in Figure 4 for comparison. The results suggest that, as a first approximation (conceptually presented in Figure 5), the bone spicules can be viewed as an ensemble of spheres with a diameter equal to the mean path length $\bar{l}_b$ of the lesion samples. If we consider spheres as a special case of ellipsoids with degenerate semi-axes (p = q = r), the next order of approximation would be an ensemble of ellipsoids with semi-axes: $p_i \neq q_i \neq r_i$ (in general) for the ith ellipsoid.

The dimensions of the semi-axes p_i, q_i and r_i could then be determined from the three path lengths l_{pi}, l_{qi} and l_{ri} sampled from the bone path-length distribution $f_b(l)$ (Fig. 5C) according to:
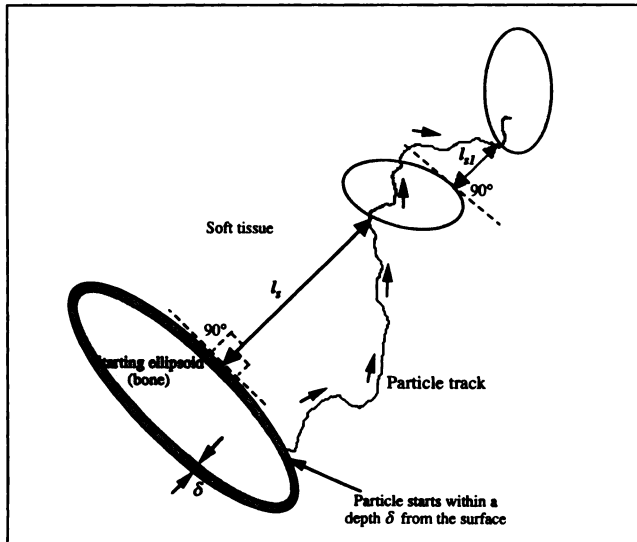
$$p_i = \frac{l_{pi}}{2}, \quad q_i = \frac{l_{qi}}{2}, \quad r_i = \frac{l_{ri}}{2}.$$

However, with the goal of minimized computational overhead associated with geometry calculations in EGS4 subroutines (HOWFAR and HOWNEAR in our model) we have used prolate and oblate ellipsoids with semi-axes $p_i = q_i \neq r_i$. A prolate ellipsoid with $p_i > r_i$ has a plate like geometry (flying saucer), while an oblate ellipsoid with $p_i < r_i$ has a rod-like geometry with tapering ends.

For a large number N of sampled (simulated) ellipsoids, the ratio $[A_b/V_b]_{sim}$ is computed according to:

$$\left[\frac{A_b}{V_b}\right]_{sim} = \frac{\displaystyle\sum_i^N a_i(p_i, r_i)}{\displaystyle\sum_i^N v_i(p_i, r_i)}, \qquad \text{Eq. 21}$$

where $a_i(p_i, r_i)$ is the surface area of the ith ellipsoid and $v_i(p_i, r_i)$ is the volume of the ith ellipsoid, is found to obey the approximate relationship (Fig. 6):

TABLE 3
Elemental Compositions of Soft Tissue and Bone Used in the Monte Carlo Simulation

Medium	Elemental composition (percentage by mass)	Density (ρ) kg m^{-3}
Soft tissue (skeleton-red marrow, adult (24))	H: 10.5, C: 41.4, N: 3.4, O: 43.9, P: 0.1, S: 0.2, Cl: 0.2, K: 0.2, Fe: 0.1	1030
Bone (skeleton-humerus, adult (24))	H: 6.0, C: 31.4, N: 3.1, O: 36.9, Na: 0.1, Mg: 0.1, P: 7.0, S: 0.2, Ca: 15.2	1460

$$\left[\frac{A_b}{V_b}\right]_{sim} \approx k_{sim} \cdot \bar{l_b}^{-n} \quad (k_{sim} = 4.2,\ n = 1.04). \qquad \text{Eq. 22}$$

The resulting $[A_b/V_b]_{sim}$ values are, however, still greater than those of the actual samples. Further refinement of the model with simulation biased towards either prolate or oblate ellipsoids or with axes $p_i \neq q_i \neq r_i$ remains to be investigated.

Radiation Transport in a Soft-Tissue Medium with Randomly Distributed Bone Spicules. The conceptual framework for the simulation of radiation transport in a multiple bone-spicule environment is based on the ensemble sampling of radiation emission from a randomly picked bone-spicule (starting ellipsoid) in an infinite sample volume and the consequent radiation transport in soft-tissue spaces where bone spicules (intercepting ellipsoids) are encountered randomly by the transported particles.

The starting and intercepting bone ellipsoids are modeled with dimensions sampled from the bone path length distribution $f_b(l)$ as described previously. Radiation traversing the soft tissue spaces is constrained using path lengths sampled from the soft tissue path length distribution $f_s(l)$. The model based on these concepts is depicted in Figure 7 and the algorithmic implementation is outlined in Appendix A.

A radiation particle from the ^{186}Re spectrum is started within a depth δ of a starting ellipsoid. A distance l_s, sampled from $f_s(l)$ is used as the limiting distance the particle can travel in soft tissue as follows: if, during transport, the particle leaves the starting ellipsoid and reaches a perpendicular distance l_s in soft tissue from the starting ellipsoid (Fig. 7), then the particle is assumed to enter an intercepting ellipsoid which then is randomly sampled. The point and direction of entry with respect to the intercepting ellipsoid are also randomly sampled. A new soft tissue path length l_{s1} now

constrains the soft tissue space surrounding this ellipsoid, until yet another intercepting ellipsoid is encountered. This process is iterated for succeeding intercepting ellipsoids until the particle transport is terminated. After completing a given number NHIST_ STARTING_ELLIPSOID (see Appendix) of transport histories in this manner from the starting ellipsoid, a new starting ellipsoid is sampled, and the process is repeated until a minimum number of $n = 100,000$, (Appendix A) particle transport histories are completed.

The mean ranges of the beta minus particles and of the conversion electrons from ^{186}Re are less than a millimeter in soft tissue and bone. Therefore, for typical lesion volumes greater than a few cubic centimeters, the infinitely large sample criterion is satisfied except for bone spicules located near the lesion surface. Any resulting error was assumed to be negligible.

In addition to the absorbed fraction in soft tissue $\phi_{s\leftarrow b}$, the absorbed fraction in bone $\phi_{b\leftarrow b}$, is also evaluated in the Monte Carlo simulation. The absorbed fraction $\phi_{b\leftarrow b}$ in bone, can be resolved into two components:

$$\phi_{b\leftarrow b} = {}^{self}\phi_{b\leftarrow b} + {}^{ext}\phi_{b\leftarrow b}, \qquad \text{Eq. 23}$$

where $^{self}\phi_{b\leftarrow b}$ is the fraction of energy deposited by particles in their originating bone spicules (starting ellipsoids) and $^{ext}\phi_{b\leftarrow b}$ is the fraction of energy deposited by particles in bone spicules external to the originating spicules (intercepting ellipsoids).

The elemental compositions of red marrow (adult) and skeleton (adult humerus), obtained from ICRU Report 46 (24) (Table 3), were used for soft tissue and bone, respectively, to generate (using PEGS4 software) the media data (reaction cross sections, etc.) files required by EGS4.
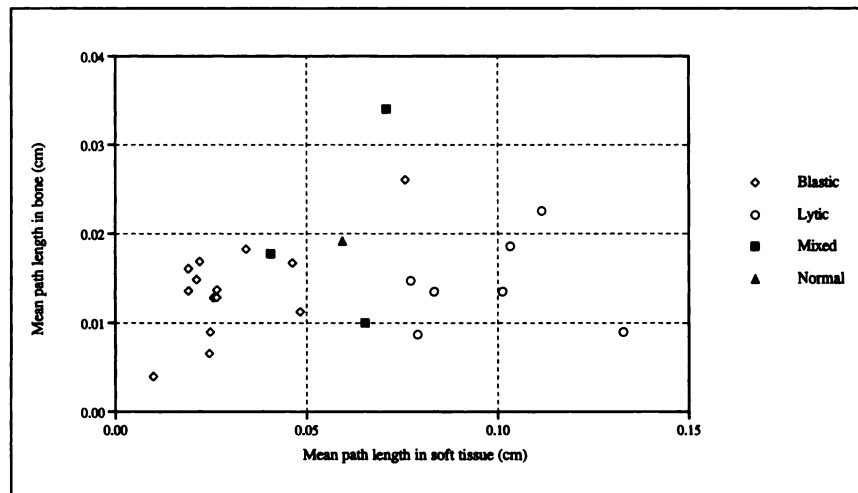
FIGURE 8. Mean path lengths in soft-tissue (l_s) and bone (l_b) components of lesion samples (n = 25).
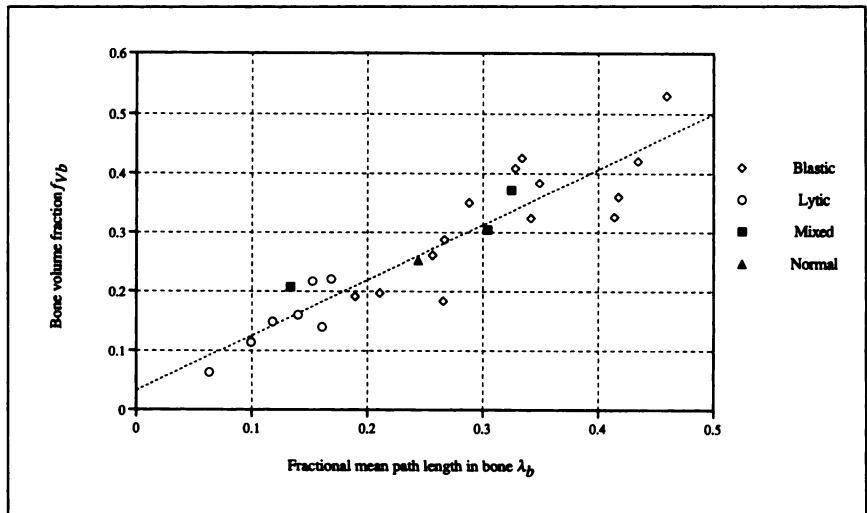
FIGURE 9. Bone volume fraction f_{Vb} as a function of fractional mean path length λ_b in bone (n = 25). The dashed line represents a linear regression curve fit (y = 0.934x + 0.033).

RESULTS

Autoradiography

The Magiscan image analysis showed deposition on bone spicules up to a depth δ of approximately 10 μm for all seven patient biopsies. The analysis showed that ratio a_s/a_{tot} (Eq. 1) was consistent with unity although there were uncertainties associated with anomalous optical density artifacts and the estimation of background optical densities. For the purpose of Monte Carlo simulations, this ratio was taken to be unity which provides the justification for the model assumption that $\tau_s = 0$ and $\tau_b = \tau_l$ as described previously.

Histomorphometry

As shown in Table 1, the mean path lengths $\bar{l}_s$ in soft tissue varied from ~0.01 to ~0.13 cm and the mean path lengths $\bar{l}_b$ in bone ranged from ~0.004 to ~0.034 cm. As shown in Figure 8 there is no apparent correlation between the mean path lengths $\bar{l}_s$ and $\bar{l}_b$. However, in general, the lytic lesions had long soft tissue path lengths $\bar{l}_s$, high path

length ratios $\bar{l}_s/\bar{l}_b$ and vice versa for blastic lesions. The three mixed lesions and the normal sample had intermediate values. The bone volume fraction f_{Vb} shows an approximately linear dependence on the fractional mean bone path length $\lambda_b = \bar{l}_b/(\bar{l}_b + \bar{l}_s)$ as shown in Figure 9. Bone surface per unit bone volume $[S_b/V_b]$ is approximately, inversely related to the mean path length in bone as shown in Figure 4. As discussed previously, this dependence as illustrated in Figure 4 was the basis for the geometry model used for the bone spicules in lesions.

Monte Carlo Simulation: Absorbed Fractions in Soft Tissue and Bone

For each of the 25 samples, radionuclide deposition depths of 0.0 and 10 μm on bone-spicule surfaces were simulated. The Monte Carlo simulation results for bone surface-to-bone volume ratio are shown in Figure 6. Correlations of the absorbed fractions in bone and soft tissue with various sample parameters were investigated. Clearly evident correlations are presented in Figures 10, 11, 12 and
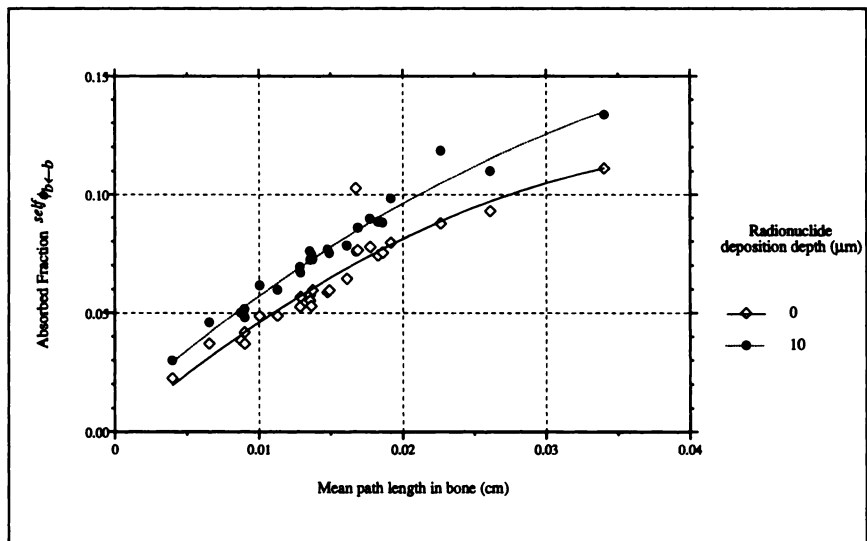
FIGURE 10. Absorbed fraction $^{self}\phi_{b\leftarrow b}$ in starting ellipsoids as a function of mean path length $\bar{l}_b$ in bone of metastatic lesions (n = 25). Solid line is the quadratic curve fit to 0 μm deposition depth results. Dashed line is the quadratic curve fit to 10 μm deposition depth results.
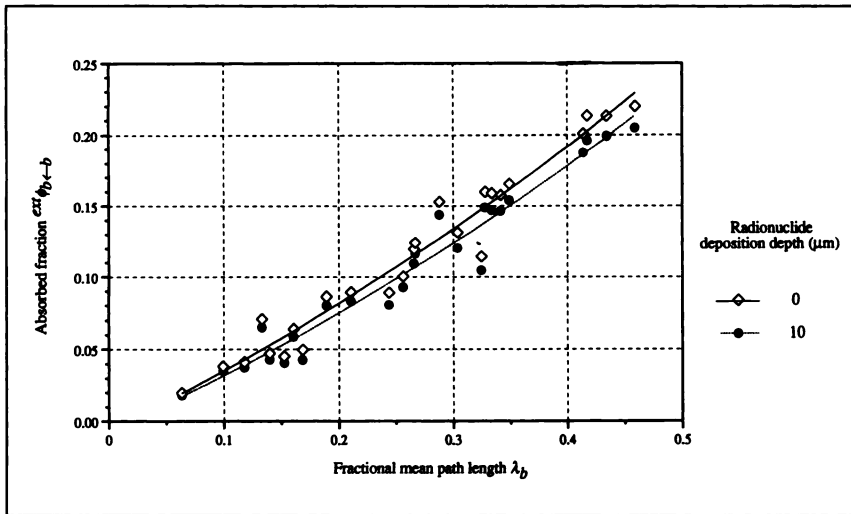
FIGURE 11. Absorbed fraction $^{ext}\phi_{b\leftarrow b}$ in intercepting ellipsoids as a function of the fractional mean path length λ_b in bone of metastatic lesions (n = 25). Solid line is the quadratic curve fit to 0 μm deposition depth results. Dashed line is the quadratic curve fit to 10 μm deposition depth results.

13 with linear or quadratic curve fits as aids to visualize these relationships. No physical significance is attached to the polynomial coefficients of these curve fits. The results are also summarized in terms of average values and standard deviations for each lesion type in Table 4.

A quadratic curve fit to the absorbed fraction in starting ellipsoids, $^{self}\phi_{b\leftarrow b}$, demonstrated a monotonically increasing dependence on the mean path length $\bar{l}_b$ in bone, as shown in Figure 10. Since $\bar{l}_b$ is representative of the average ellipsoid (bone-spicule) dimension, absorbed fractions in starting ellipsoids increase with increasing bone-spicule size as expected. In the case of the intercepting ellipsoids, the absorbed fraction $^{ext}\phi_{b\leftarrow b}$ exhibited a monotonically increasing dependence on the fractional mean path length, $\lambda_b = \bar{l}_b/(\bar{l}_b + \bar{l}_s)$ in bone as shown in Figure 11.

As the radionuclide deposition depth δ into the bone spicules increases, the absorbed fraction, $^{self}\phi_{b\leftarrow b}$, increases in the starting ellipsoids with the increase being correspondingly bigger for larger bone spicules (Fig. 10) as expected. In addition, the intercepting ellipsoids show a

small but consistently decreased absorbed fraction $^{ext}\phi_{b\leftarrow b}$ (Fig. 11) with increasing δ as a result of less radiation energy being transported to the intercepting ellipsoids.

The absorbed fraction $\phi_{s\leftarrow b}$ in soft tissue exhibits an approximately linear dependence on the fractional mean path length in soft tissue $\lambda_s = \bar{l}_s/(\bar{l}_b + \bar{l}_s)$ (Fig. 12). With increasing δ, the absorbed fraction in soft tissue decreases as expected. The average decrease (excluding one anomalous data point) with respect to $\phi_{s\leftarrow b}$ for $\delta = 0$, was 1.5% with a range of 0.9% to 3.1%. Since the fractional mean path length in bone λ_b is linearly related to the bone volume fraction f_{Vb} (Fig. 9) and $\lambda_s = 1 - \lambda_b$, the absorbed fraction $\phi_{s\leftarrow b}$ also shows a linear dependence on f_{Vb} with a negative slope (Fig. 13).

DISCUSSION

Dosimetry

The objective of the current investigation is to establish more realistic radiation dose estimates to bone metastases
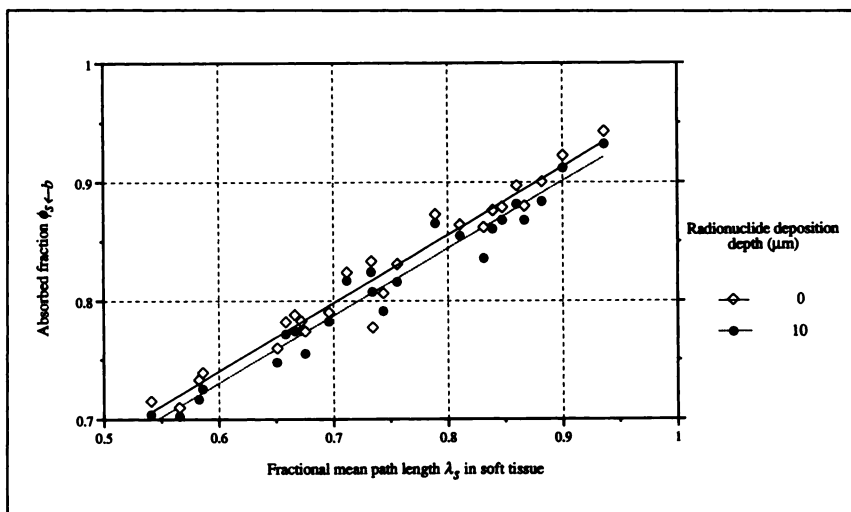
FIGURE 12. Absorbed fraction $\phi_{s\leftarrow b}$ in soft tissue as a function of fractional mean path length λ_s in soft tissue of metastatic lesions (n = 25). Solid line is the linear curve fit to 0 μm deposition depth results. Dashed line is the linear curve fit to 10 μm deposition depth results.
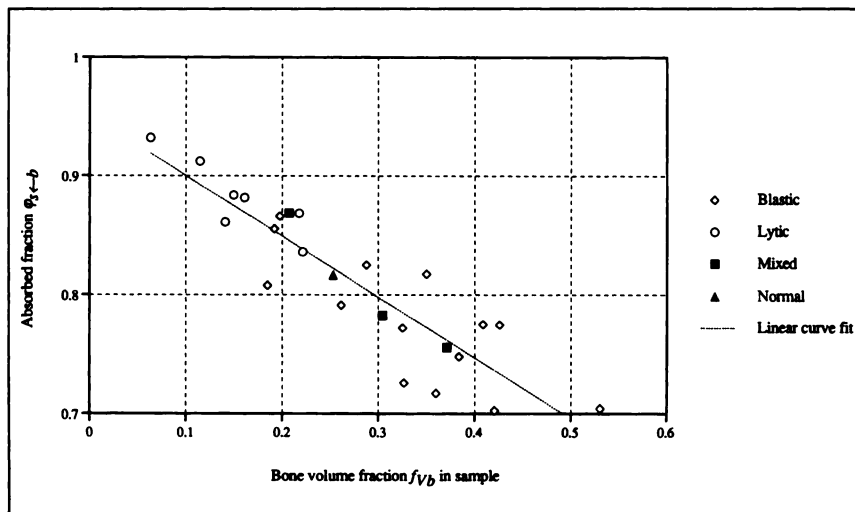
FIGURE 13. Absorbed fraction $\phi_{s\leftarrow b}$ in soft tissue for 10 μm radionuclide deposition depth in bone as a function of bone volume fraction f_{Vb} of lesion samples (n = 25). Dashed line is the linear curve fit to data.

through a model which incorporates the tumor soft tissue configuration within a trabecular bone-like environment characterized by radiopharmaceutical uptake near the bone spicule surface. The Monte Carlo simulations described above have provided soft tissue (tumor) absorbed fractions, $\phi_{s\leftarrow b}$, for [186]Re deposited on or to a depth of 10 μm from the bone surface for this histomorphometrically heterogenous small scale geometry. In contrast, the commonly employed uniform lesion model assumes tumor absorbed fractions of unity for charged particles in the [186]Re spectrum.
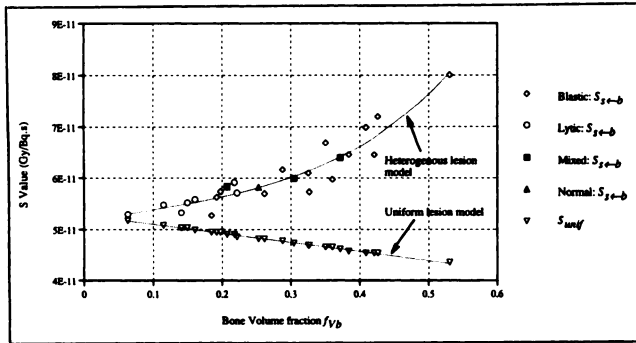
As stated in Equation 9, the dose to the tumor soft tissue is obtained from the product of the S value and the lesion residence time τ_l. Thus, per previous discussion, for a given τ_l (determined experimentally in vivo through sequential quantitative measurements of lesion activity, $a_l(t)$), the relative dose from the two models may be evaluated through comparison of the respective S values.

S Values: Uniform Lesion Model (S_{unif}) and Heterogenous Lesion Model ($S_{s\leftarrow b}$)

S values for both models based on Equations 17 and 18 and normalized to a 1-cm^3 volume are shown in Figure 14 and listed in Table 5. The tissue densities used for these calculations are shown in Table 3 and correspond to the media used in the Monte Carlo simulation. The heterogenous model S value $S_{s\leftarrow b}$ increases by a factor of ~1.5 over the bone volume fraction range of ~0.06 to ~0.53; i.e., blastic lesions with generally high bone volume content or equivalently high lesion density have larger S values than lytic lesions with low bone content. As shown in Figure 13, the soft tissue absorbed fraction ϕ_s decreases from ~0.9 to ~0.7 with increasing bone volume fraction. However, as the bone volume fraction increases, the accompanying decrease in the mass of soft tissue component in the lesion ($\rho_s \cdot f_{Vs}$ in the denominator of Equation 18) results in high $S_{s\leftarrow b}$ for lesions with high bone volume fraction. For lytic

TABLE 4
Monte Carlo Simulation Results

Absorbed fractions ϕ for charged particles in the [186]Re spectrum

$\phi_{s\leftarrow b}$: soft tissue

$^{self}\phi_{b\leftarrow b}$: starting ellipsoids

$^{cxt}\phi_{b\leftarrow b}$: intercepting ellipsoids

$\phi_{b\leftarrow b} = {}^{self}\phi_{b\leftarrow b} + {}^{cxt}\phi_{b\leftarrow b}$

Histologic type/no. of samples		0 μm deposition depth in bone				10 μm deposition depth in bone (surface deposition)			
		$\phi_{s\leftarrow b}$	$^{self}\phi_{b\leftarrow b}$	$^{cxt}\phi_{b\leftarrow b}$	$\phi_{b\leftarrow b}$	$\phi_{s\leftarrow b}$	$^{self}\phi_{b\leftarrow b}$	$^{cxt}\phi_{b\leftarrow b}$	$\phi_{b\leftarrow b}$
Blastic/14	Average	0.785	0.060	0.154	0.215	0.777	0.070	0.152	0.223
	s.d.	0.051	0.021	0.046	0.051	0.053	0.020	0.045	0.053
Mixed/3	Average	0.815	0.079	0.106	0.185	0.802	0.095	0.103	0.198
	s.d.	0.057	0.031	0.031	0.057	0.059	0.036	0.030	0.059
Normal/1		0.831	0.080	0.089	0.169	0.816	0.098	0.085	0.184
Lytic/7	Average	0.897	0.059	0.044	0.103	0.882	0.076	0.042	0.118
	s.d.	0.028	0.018	0.013	0.028	0.032	0.024	0.013	0.032

FIGURE 14. S values for the (i) heterogenous $S_{s \leftarrow b}$ and (ii) uniform S_{unif} lesion models as a function of the bone volume fraction f_{vb} of lesion samples (n = 25). Radionuclide deposition depth in bone is 10 μm. Dashed lines are drawn as guides to the eye to identify the two models.

lesions with small bone volume fractions, the heterogenous model approaches the characteristics of the uniform model resulting in similar S value estimates for both models. The uniform model is seen to underestimate the dose for blastic lesions, by factors ranging from 1.07 to 1.84 with an average value of 1.35 ± 0.2 (Table 5). The uniform model also underestimates the doses to mixed lesions by factors ranging from 1.19 to 1.39 (average: 1.29 ± 0.1).

The extensive input data required for the Monte Carlo simulation of the heterogenous lesion model cannot be obtained routinely under clinical conditions. However, the strong dependence of $S_{s \leftarrow b}$ on the bone volume fraction of the lesion (Fig. 14), suggests that the S value based on Monte Carlo results can be empirically reduced to a dependence on lesion density which in turn can be determined through quantitative x-ray computed tomography (XCT) measurements. However, given $S_{s \leftarrow b}$, the actual residence time τ_l in a given lesion is required for the determination of dose to lesion D_s (= $S_{s \leftarrow b} \cdot \tau_l$). As pointed out previously, the actual residence time for a given lesion depends on patient-specific factors such as the lesion volume, uptake and the time scales of biologic turnover.

CONCLUSIONS

We have developed a geometric model and a radiation transport algorithm that can be used in the Monte Carlo simulation of dose delivery to skeletal metastases by bone-seeking radiopharmaceuticals. The simulation incorporates the actual geometric characteristics of skeletal metastases as obtained from histomorphometric techniques; the radiopharmaceutical deposition patterns in the metastatic lesion as evidenced from autoradiographic data; and the radiation spectrum of the radionuclides. For [186]Re-HEDP, the results show that the S value, $S_{s \leftarrow b}$, for metastatic skeletal lesions increases with increasing bone volume fraction, or equivalently, with increasing lesion density. Consequently, the dose to the tumor (soft tissue) will be higher for this realistic heterogenous model than that estimated by the commonly used uniform lesion model. This new knowledge is imperative for optimal treatment planning and dose response evaluations (patient outcome and toxicity). This new model should be applicable to other bone-seeking beta-emitting radionuclides such as [188]Re, ^{90}Y, ^{89}Sr, [153]Sm and [117m]Sn which also are presently in clinical use or under investigation for the treatment of skeletal metastases.

APPENDIX

An Algorithm for the Simulation of Charged Particle Transport in a Matrix of Bone Ellipsoids Embedded Randomly in Soft Tissue Using EGS4 Monte Carlo Transport System

The simulation is based on EGS4/PRESTA (20,21) Fortran code system for Monte Carlo simulation of coupled transport of electrons and photons. Transport for particles with energies between a few kiloelectron volts and several teraelectron volts can be simulated in media with arbitrary geometry. The particle type, initial energy, location and direction; geometry of the transport environment; and media (elemental composition by weight) are specified by user-written software and data.

Typically, control is passed to EGS4 from a user-written main program to initiate particle transport. Subsequently, at various stages during the transport, EGS4 communicates with user-written subroutines, HOWFAR and HOWNEAR, to obtain geometry

TABLE 5
Summary of [186]Re S Values Normalized to a 1-cm^3 Lesion Volume for 25 Metastatic Lesion Samples

Histologic type/no. of samples		S value (Gy/Bq s) uniform lesion model S_{unif}	S value (Gy/Bq s) hetero. lesion model (Monte Carlo) $S_{s \leftarrow b}$	S value ratio $S_{s \leftarrow b}/S_{unif}$ (=dose ratio)*
Blastic/14	Average	4.69×10^{-11}	6.30×10^{-11}	1.35
	s.d.	0.17×10^{-11}	0.73×10^{-11}	0.21
Mixed/3	Average	4.75×10^{-11}	6.08×10^{-11}	1.28
	s.d.	0.15×10^{-11}	0.29×10^{-11}	0.10
Normal/1		4.821×10^{-11}	5.824×10^{-11}	1.21
Lytic/7	Average	5.01×10^{-11}	5.56×10^{-11}	1.11
	s.d.	0.11×10^{-11}	0.21×10^{-11}	0.07

*For a common lesion residence time, the dose ratio for the two models is equivalent to the S value ratio.

information regarding media boundaries. User-written subroutine AUSGAB captures information generated by EGS4 regarding energy deposition, particle location, etc., during transport.

The algorithmic description given below is implemented in conjunction with EGS4. Photons from the [186]Re spectrum and Bremsstrahlung production from the low-energy negative beta particles are discarded (ignored) in this implementation. Mechanisms/conventions for discarding particles, output of simulation information etc., are well documented by EGS4 and therefore not described. EGS4 transports a charged particle in small steps USTEP at a time, in conjunction with subroutines HOWFAR and HOWNEAR. Before evaluating the magnitude and direction of a USTEP to be transported, EGS4 queries HOWNEAR for the perpendicular distance TPERP from the current location of the particle to the nearest region boundary. TPERP is used by EGS4 in determining the magnitude of USTEP for charged particles in the close proximity of media boundaries (boundary-crossing algorithm in PRESTA). After evaluating USTEP, EGS4 calls HOWFAR to determine whether the planned USTEP would occur across a media boundary. If a media boundary will be crossed, HOWFAR shortens the requested USTEP to the boundary and informs EGS4 about the boundary crossing into a new region through the global variable IRNEW.

LOOP1, LOOP2 and LOOP3 (see below) identify nested iterations at increasing levels of depth in the algorithm. Geometry for the starting ellipsoid (initial geometry), and the number of histories to be started from this ellipsoid, are set up in LOOP1. Particle transport begins at the nesting level of LOOP2; i.e., control is passed to EGS4 at this level by calling the SUBROUTINE SHOWER. Subsequently, as the particle is transported by EGS4, it encounters intercepting ellipsoids randomly in LOOP3. LOOP3 is not explicitly constructed in the software as shown but indicates the effective flow path in the pseudo code when EGS4 runs in conjunction with the user-written subroutines HOWFAR and HOWNEAR. LOOP3 also behaves like an indefinite loop until EGS4 terminates the particle transport. Transfer of pseudo code execution from EGS4 to subroutines HOWNEAR and HOWFAR in LOOP3 are indicated by entry points ENTRY 1 and ENTRY 2, respectively. Similarly, flow of execution back to EGS4 from these subroutines is indicated by the exit points, RETURN1 and RETURN2, respectively. EGS4 is also greatly simplified within LOOP3 to a few pseudo code statements and comments, relevant to the transport algorithm. The reader is referred to reference 13 for a comprehensive look at the flow charts of EGS4. Boundary-locating algorithms required in HOWFAR and HOWNEAR are also not presented but their use is implicit in the pseudo code statements in LOOP3.

STARTING_ELLIPSOID, INTERCEPTING_ELLIPSOID, and CURRENT_ELLIPSOID are identifiers for data structures that describe ellipsoids. To accommodate a shower of particles (delta rays, etc.) arising from the original particle, EGS4 maintains last in first out (LIFO) stack variables for the particle position, energy, etc., using a stack pointer variable NP. EGS4 increments/ decrements NP when a shower particle is created/terminated. Therefore, to accommodate the random encounter of ellipsoids in LOOP3 by the daughter particles in the shower, the CURRENT_ ELLIPSOID is also maintained in a LIFO stack using the stack pointer NP.

A major drawback in the algorithm, as will be seen below, is that the absolute location of the transported particle, with respect to the starting ellipsoid, cannot be tracked once an intercepting ellipsoid is encountered. This is due to shifting of the coordinate

reference frame as each new intercepting ellipsoid is encountered. However, the information of primary interest; i.e., the fraction of the energy ϕ absorbed in the ellipsoids (starting and intercepting) and soft tissue after a sufficient number of transport histories are completed, can still be obtained by tracking the energy deposited in the respective regions. Another inherent assumption in this algorithm is that after a particle encounters an intercepting ellipsoid, it does not return to the starting ellipsoid. This does not introduce a conceivable error in the estimation of ϕ_b deposited in the totality of the bone ellipsoids (starting + intercepting), but does introduce an error in how it is apportioned between the starting and intercepting ellipsoids ($^{self}\phi_{b\leftarrow b}$, and $^{ext}\phi_{b\leftarrow b}$). This error is assumed negligible.

The Algorithm (Comments Are in Italics)

Initialize: NHIST = 0
Geometric region identifiers:
SOFT_TISSUE = 1 (soft tissue)
BONE1 = 2 (starting ellipsoid)
BONE2 = 3 (intercepting ellipsoids)
.....
Read:
(1) Path length distributions: $f_b(l)$, and $f_s(l)$ for lesion sample
(2) Re186-Spectrum data
(3) Media data: Reaction cross sections etc.
Assign:
(1) DELTA: Depth of uniform deposition of radionuclides on bone-spicule surfaces
(2) NHIST_PER_AREA: number of particle histories to be started per unit area of bone surface within lesion
(3) N: Minimum number of particle transport histories to be executed
N = 100,000 was used for all lesion sample simulations.
LOOP1: DO WHILE (NHIST < N)
Sample an ellipsoid from which the radiation emissions are started
Sample two path lengths in bone: LA, and LB from $f_b(l)$
Ellipsoid axes: A = B = LA/2 and C = LB/2
STARTING_ELLIPSOID = [A,B,C]
All possible daughter particles in the shower initially inherit the same geometric environment. 'J' refers to the LIFO stack index.
DO J = 1, NP_MAX (NP_MAX: maximum depth of shower stack)
CURRENT_ELLIPSOID[J] = STARTING_ELLIPSOID
END DO
INTERCEPTED_ELLIPSOIDS = FALSE, initialize as FALSE. Intercepting ellipsoids have not been encountered yet.
Number of particles (histories) started from this ellipsoid. Evaluate ellipsoid surface area: AREA_ELLIPSOID
NHIST_STARTING_ELLIPSOID = AREA_ELLIPSOID* NHIST_PER_AREA
LOOP2: DO (K = 1, NHIST_STARTING_ELLIPSOID)
If previous particle intercepted ellipsoids then restore the geometry.
IF(INTERCEPTED_ELLIPSOIDS) THEN
DO J = 1, NP_MAX (NP_MAX: maximum depth of shower stack)
CURRENT_ELLIPSOID[J] = STARTING_ELLIPSOID

END DO
END IF
A decay particle is sampled from starting ellipsoid.
Sample energy E0 and particle type PTYPE: From Re-186 Spectrum.
Sample direction K0: [U0, V0, W0]: From isotropic distribution.
Sample location R0: [X0, Y0, Z0]: From uniform volume distribution up to a depth DELTA from the surface of CURRENT_ELLIPSOID.
Sample LS from $f_s(l)$: Sample the limiting distance LS in soft tissue (perpendicular distance from the CURRENT_ELLIP-SOID surface) this particle will be allowed to travel.
ENTERING_INTERCEPTING_ELLIPSOID = FALSE
Initiate particle transport by transferring control to EGS4.
Particle starts with values: E0, X0,.. U0,.. in region: BONE1 (starting ellipsoid).
CALL SHOWER (PTYPE, E0, X0,.. U0,.. BONE1,...)
Particle transport in multiple bone spicule environment:
LOOP3: *Indefinite. Exits when EGS4 terminates particle transport.*
    Begin/continue transport in EGS4.
    .....
    CALL HOWNEAR (before evaluating the next USTEP)
    ENTRY 1: (into HOWNEAR from EGS4)
    IF (ENTERING_INTERCEPTING_ELLIPSOID)
        Sample INTERCEPTING_ELLIPSOID from $f_b(l)$.
        With respect to the new ellipsoid:
        Sample random point of entry on surface: R' = [RX,RY,RZ]
        Sample random direction into the ellipsoid: K' = [KX,KY,KZ]
        Change the variables corresponding to (i) position and (ii) direction for the particle at the top of the shower stack. Reference frame is now with respect to the new ellipsoid.
        X[NP] = RX, Y[NP] = RY, Z[NP] = RZ
        U[NP] = KX, U[NP] = KY, W[NP] = KZ
        Sample a soft tissue distance LS from $f_s(l)$ (the limiting distance)
        The current ellipsoid is accessed in HOWFAR using the stack pointer NP. Therefore, make sure the daughter particles in the shower from this point on will have this new geometric environment.
        DO K = NP,NP_MAX
            CURRENT_ELLIPSOID[K] = INTERCEPTING_ELLIPSOID
        END DO
        INTERCEPTED_ELLIPSOID = TRUE *Alert LOOP2 to restore the geometry when the next particle is started*
        ENTERING_INTERCEPTING_ELLIPSOID = FALSE
    END IF
    Evaluate TPERP
    RETURN 1 *(Exit HOWNEAR and return to EGS4)*
    Evaluate USTEP

    .....
    CALL HOWFAR *(before transporting the USTEP)*
    ENTRY 2: *(into HOWFAR from EGS4)*
    IF (particle is in SOFT_TISSUE) THEN
        IF (perpendicular distance D from CURRENT_ELLIP-SOID[NP] surface after taking USTEP is greater than or equal to LS) THEN

adjust USTEP such that D = LS
            ENTERING_NEW_ELLIPSOID = TRUE
            IRNEW = BONE2 *(intercepting ellipsoid)*
        .....
        ELSE
            Particle might cross into the current ellipsoid etc. Handle USTEP accordingly.
        .....
        END IF
    ELSE *Particles is in a bone region (inside an ellipsoid). Handle USTEP accordingly.*
    .....
    END IF
    RETURN 2 *(Return to EGS4)*
    transport particle by USTEP

    .....
    IF (the particle energy falls below cutoff energy ECUT) THEN
        terminate transport and exit LOOP3
    END IF

    .....
    GOTO LOOP3
End LOOP3
Shower is terminated. Restore original geometry before starting next shower.
DO K = 1, NP_MAX
    CURRENT_ELLIPSOID[K] = STARTING_ELLIPSOID
END DO
End LOOP2: END DO
NHIST = NHIST + NHIST_STARTING_ELLIPSOID
End LOOP1: END DO *(Finished with this starting ellipsoid.)*
    Finish simulation.

In the conventional usage of EGS4, the routines HOWFAR and HOWNEAR are written for predetermined geometries that do not change during program execution. However, in the algorithm described above, the geometries are determined randomly during particle transport, and the flow structure of EGS4 can accommodate this random geometry creation as shown above. HOWFAR determines when the particle is about to enter a new intercepting ellipsoid and sets the status of the global logical variable ENTERING_NEW_ELLIPSOID to TRUE and passes control to EGS4. HOWNEAR is then called by EGS4 before executing a particle step in the new region. HOWNEAR creates a new geometry environment depending on the status of the global variable ENTERING_NEW_ELLIPSOID; assigns the new R' and K' values to the current particle being transported; and evaluates TPERP which would be zero in this case and returns control to EGS4. The above scheme does not work when Bremstrahlung production occurs in a shower since HOWNEAR is accessed by EGS4 only for charged particle transport. To get around this difficulty, photons are discarded in the present implementation as mentioned previously. However, Dr. D.W.O. Rogers (National Research Council of Canada) has suggested *(personal communication, July 1993)* a solution which will be implemented in a future refinement of the above algorithm.

REFERENCES

1. Tong D, Gillick L, Hendrickson FR. The palliation of symptomatic osseous metastases: final results of the study by the radiation therapy oncology group. *Cancer* 1982;50:893–899.
2. Robinson RG. Editorial: systemic radioisotopic therapy of primary and metastatic bone cancer. *J Nucl Med* 1990;31:1326–1327.
3. Maxon HR, Schroeder LE, Thomas SR, et al. Radionuclide palliation of cancer-related bone pain. In: McCartney, ed. *Current clinical role of nuclear medicine: comparison with other modalities*. Cincinnati, OH: Southeastern Chapter of the Society of Nuclear Medicine; 1988;17:2–18.
4. Ketring AR. Samarium-153-EDTMP and ^{186}Re-HEDP as bone therapeutic radiopharmaceuticals. *Nucl Med Biol* 1987;14:223–232.
5. Maxon HR III, Thomas SR, Hertzberg VS, et al. Rhenium-186-hydroxyethylidene diphosphonate for the treatment of painful osseous metastases. *Semin Nucl Med* 1992;22:33–40.
6. Goeckler WF, Edwards B, Volkert WA, Holmes RA, Simon J, Wilson D. Skeletal localization of samarium-153 chelates: potential therapeutic bone agents. *J Nucl Med* 1987;28:495–504.
7. Collins C, Eary JF, Donaldson G, et al. Samarium-153 EDTMP in bone metastases of hormone refrectory prostate carcinoma: a phase I/II trial. *J Nucl Med* 1993;34:1839–1844.
8. Eisenhut M, Berberich R, Kimmig B, Oberhausen E. Iodine-131-labeled diphosphonates for palliative treatment of bone metastatses: II. Preliminary clinical results with iodine-131-BDP3. *J Nucl Med* 1986; 27:1255–1261.
9. Robinson RG, Preston DF, Spicer JA, Baxter KG. Radionuclide therapy of intractable bone pain: emphasis on strontium-89. *Semin Nucl Med* 1992;22: 28–32.
10. Aziz H, Choi K, Sohn C, Yaes R, Rotman M. Comparison of ^{32}P therapy and sequential hemibody radiation (HBI) for bony metastases as methods of whole-body irradiation. *Am J Clin Oncol* 1986;9:264–268.
11. Kutzner J, Dahnert W, Schreyer T, Grimm W, Brod KH. Yttrium-90 zur schmerztherapie von knochenmetastasen. *Nuclearmedizin* 1981;20:229–235.
12. Srivastava SC, Meinken GE, Richards P, et al. The development and in vivo behaviour of tin containing radiopharmaceuticals: chemistry, preparation and biodistribution in small animals. *Int J Nucl Med Biol* 1985;3:167–174.
13. Whitwell JR, Spiers FW. Calculated beta-ray dose factors for trabecular bone. *Phys Med Biol* 1976;21:16–38.
14. Beddoe AH, Darley PJ, Spiers FW. Measurement of trabecular bone structure in man. *Phys Med Biol* 1976;21:589–607.
15. Spiers FW, Beddoe AH. Radial scanning of trabecular bone: consideration of the probability distributions of path lengths through cavities and trabeculae. *Phys Med Biol* 1977;22:670–680.
16. Spiers FW, Whitwell JR, Beddoe AH. Calculated dose factors for the radiosensitive tissues in bone irradiated by surface-deposited radionuclides. *Phys Med Biol* 1978;23:481–494.
17. Parfitt AM. Stereologic basis of bone histomorphometry: theory of quantitative microscopy and reconstruction of the third dimension. In: Becker RR, ed. *Bone histomorphometry: techniques and preparation*. Boca Raton, Florida: CRC Press, Inc; 1983:53–87.
18. Loevinger R, Budinger TF, Watson EE in collaboration with MIRD Committee. *MIRD primer for absorbed dose calculations*. New York: Society of Nuclear Medicine; 1988.
19. Thomas SR, Maxon HR, Kereiakes JG. In vivo quantitation of lesion radioactivity using external counting methods. *Med Phys* 1976;3:253–255.
20. Nelson WR, Hirayama H, Rogers DWO. *The EGS4 code system*, SLAC-Report-265, December 1985, Stanford Linear Accelerator Center, Stanford University, Stanford, California.
21. Bielajew AF, Rogers DWO. PRESTA, the "parameter reduced electron-step transport algorithm" for electron Monte Carlo transport. *Nucl Instr Meth* 1987;B18:165–181.
22. Prestwich WV, Nunes J, Kwok CS. Beta dose point kernels for radionuclides of potential use in radioimmunotherapy. *J Nucl Med* 1989;30:1036–1046.
23. Weber DA, Eckerman KF, Dillman LT, Ryman JC. *MIRD: radionuclide data and decay schemes*. New York: Society of Nuclear Medicine; 1989.
24. International Commission on Radiation Units and Measurements. Body tissue compositions. In: *Photon, electron, proton and neutron interaction data for body tissues*, ICRU Report 46. Bethesda, MD: ICRU; 1992:11–13.